Healing properties of implants inserted concomitantly with anorganic bovine bone. A histomorphometric human study.

(Article begins on next page)

20 April 2024

Healing properties of implants inserted concomitantly with anorganic bovine bone. A histomorphometric human study.

SCHOLARONE™
Manuscripts

Abstract

Objectives: The present prospective, randomized, double-blind study evaluated the bone-forming process of implants inserted simultaneously with anorganic-bovine-bone (ABB) in sinus grafting.

Materials and Methods: A total of 18 threaded mini-implants with Osseotite (*O*) and Nanotite *(N)* surfaces were placed in 7 patients (9 sites). After 12 months, the implants were retrieved and processed for histological analysis. A total of 18 cutting and grinding sections were investigated with bright-field light microscopy, Circularly Polarized Light Microscopy (CPLM), Confocal Scanning Laser Microscope (CSLM), and Scanning Electron Microscope (SEM) with Energy Dispersive Spectrometer (EDS).

Results: The BIC rate in native crestal bone was $62.6 \pm 0.4\%$ for *N* implants and $54.3 \pm 0.5\%$ for the *O* implants ($p = 0.001$). The collagen fiber density, as assessed by CPLM, was 79.8 ± 6.0 nm for the *N* group and 74.6 ± 4.6 nm for the *O* group ($p<0.05$). Line scan EDS starting from ABB to newly formed bone showed a decrease in calcium content and an increase of carbon while phosphorus content was constant.

Conclusions: While the *N* surface improved the peri-implant endosseous healing properties in the native bone, when compared to the *O* surface, it did not improve the healing properties in the bone-graft area.

INTRODUCTION

The rehabilitation of partially or totally edentulous patients with implant-supported prostheses with reliable long-term results has become common practice in dentistry. Maxillary sinus floor elevation, first described by Boyne and James [1], is indicated when rehabilitating the distal maxillary region, when the height of the residual bone is less than 6 mm. The classical sinus lift procedure consists of the preparation of the lateral antrostomy through the trap door and subsequent elevation of the Schneiderian membrane to form the new sinus floor. The space generated under the repositioned sinus mucosa is filled with a graft material (of animal, synthetic or cadaveric origin) alone or combined with autologous bone. Implant insertion concurrent with grafting is possible when the bone height is deemed adequate for primary stability [2,3]. Otherwise, the implants are inserted at a second stage. Several reviews concluded the following: i) bone substitutes appear to be as effective as autologous bone grafts for augmenting atrophic maxillary sinuses [4]; ii) implant survival rates compared favorably with reported survival rates for implants placed in the non-grafted maxilla [5]; iii) rough-surface implants yielded higher survival rates than machined-surface implants when placed in grafted sinuses [6] and iv) perforation of the sinus membrane was the most frequently reported complication [7]. Literature and clinical practice have clearly shown that implants with Osseotite surface (3i Implant Innovations, Palm Beach Gardens, FL) have excellent predictability [8] and allow faster integration times, higher bone-to-implant contact (BIC) rates [9] and higher cumulative survival rates, even in short fixtures [10] than do the machined titanium surfaces. In addition, Osseotite implants have shown higher survival rates than machined implants when used in rehabilitation treatments of the posterior maxilla [11,12]. The implants with Nanotite surface (3i Implant Innovations, Palm Beach Gardens, FL) were obtained through a discrete crystalline deposition (DCD) of CaP (nominal crystal size of 20 nm) allowing a surface coverage of approximately 50%. The suggested nanofeature size of the tightly adherent adsorbed CaP/DCD crystal is 50 to 100 nm [13, 14].

Indeed, every surface has its own nanotopography, but not all of them are endowed with significant repetitive nanostructures. A nanostructured object is defined by repetitive structures the sizes of which range between 1 and 100 nm. On the nanoscale level, a more textured surface topography increases the surface energy, which improves the surface wettability to blood and the spreading and binding of fibrin and matrix proteins [15]. Therefore, surface topography should favor cell attachment and tissue healing, particularly

directly after implantation; this is of paramount importance during the osseointegration process. A few *in vitro* studies have already shown that modulating the nanotopography of an implant surface affects bone cell behavior [16,17,18]. The effects of nanotopography on biological response are not well known for commercially available implants [15] because nanofeatures of the most important commercially available dental implants have been assessed only recently [19]. However, clinical evidence has already been provided on implant surface textures featuring the application of nanometer-scale CaP [20,21].

Several case series [22,23,24] and a systematic review [25] reported the survival rate of implants and biomaterials placed in a single-staged approach. However, to the best of our knowledge, little is known about the healing process elicited by nanosurface implants that are placed concomitantly with grafting materials in humans. Actually, prior to the present research, two histological and histomorphometric evaluations dealt with short healing periods, i.e., within three months, and they did not consider bone grafting other than the autologous one [26,27]. The aim of this histological and histomorphometric study is to evaluate the bone healing process occurring around Osseotite and Nanotite implant surfaces inserted concomitantly with anorganic bovine bone (ABB) (Geistlich Söhne AG, Wolhusen, Switzerland) after one year.

MATERIAL AND METHODS

Study design

A prospective, randomized, double-blind, histomorphometric study was performed on 7 patients (9 sites). The inclusion criteria were the following: (1) presence of either interrelated or distal maxillary edentulism with at least two missing teeth; (2) ridge height of 5 mm (as assessed by orthopantomograms); (3) no history of radiotherapy in the head and neck region; (4) no history of bone-related diseases, autoimmune-related disorders and diabetes mellitus; (5) no history of coagulation disorders; (6) non-smoking patients.

All of the patients were treated at the Prosthodontic Department of the Dental School at the University of Turin after signing a written consent. The local Ethical Committee approved the study. Threaded Osseotite and Nanotite mini-implants that were 2.18 mm in diameter and 10 mm in length were used.

Surgical protocol

Each site underwent a maxillary sinus lift using the lateral window approach described by Boyne and James [1]. After elevating the flap, the preparation of a top-hinge door in the lateral maxillary sinus wall was performed using piezosurgery (Mectron S.p.A., Carasco, Italy). This door was then pushed inward and upward together with the Schneiderian membrane to a horizontal position to form the new sinus floor. The space underneath lifted the door, and the sinus mucosa was filled with ABB. At the same time, two mini-implants were inserted into the grafted sites, one from the Nanotite group (test) and one from the Osseotite group (control), for a total of 18 implants. A random cross-location method was used to determine whether a mesial or distal position was to be assigned to either the test surface or the control surface within each site. The researchers did not know the generated identification sequence. All of the bone grafts were covered by collagen membranes (Geistlich Söhne AG, Wolhusen, Switzerland). No perforations of the Schneiderian membrane occurred nor were any complications registered. The mini-implants were removed along with the adherent bone during definitive implants placement using a customized harvester 12 months after the sinus graft procedure.

Histological processing

The 18 samples were immersed in 10% buffered formalin, than they were dehydrated in graded concentrations of ethanol and embedded in resin (Technovit 7200 VLC, Kulzer, Wehrheim, Germany). After polymerization, the specimens were sectioned along the longitudinal axis with a high-precision diamond disc at about 100 µm with a custom built sawing and grinding apparatus (TT System, TMA2, Grottammare, Italy). A total of 36 sections were obtained (two longitudinal central sections for each retrieved mini-implant). Eighteen sections were ground down to about 60 ± 10 µm and stained with acid fuchsine and toluidine blue for BIC evaluation. Among the remaining specimens, 14 sections were chosen (two for each patient treated) to be investigated under polarized light. The sections measuring 100 ± 5 µm were left unstained.

Histomorphometric analysis

All experimental sites were measured by the same investigator (T.T.) without knowing the identification of the implant group. Histomorphometry was used to evaluate the BIC rate. The investigation was conducted in a transmitted brightfield Light Microscope Axiolab (Zeiss Oberchen, Germany) connected to a high-resolution digital camera (FinePix S2 Pro, Fuji Photo Film Co. LTD. Minato-Ku, Japan). A histometric software package with image capturing capabilities (Image-Pro Plus 6.0, Media Cybernetics Inc., Bethesda, MD, USA) was used. To ensure accuracy, the software was calibrated for each experimental image using a software feature named "Calibration Wizard", which reports the number of pixels between two selected points (diameter or length of the implant). The linear remapping of the pixel numbers was used to calibrate the distance in microns.

Circularly Polarized Light Microscopy (CPLM)

Birefringence was used to evaluate the collagen fiber density (CFD) of the bone pre-matrix present in the augmented sites associated with the implants surfaces. The measurements were made in the inter-thread region of the apical portion of the implants using polarized light. Because uniform section thickness is critical for the quantitative analysis of collagen fiber orientation, 14 ground sections measuring 100 ± 5 µm in thickness were used. The CFD was evaluated using a light microscope (Axiolab, Carl Zeiss, Jena,

Germany) equipped with two linear polarizers, and two quarter-wave plates retarder arranged to produce transmitted circularly polarized light. The optical system was connected to a high-resolution CCD-IRIS digital camera (Sony DXC-107-A. Tokyo, Japan) and the images were captured using an image processing software (Image-Pro Plus 6.0, Media Cybernetics Inc., Bethesda, MD, USA)

Basic principles for birefringence measurements

Birefringence is the optical technique of measuring orientation in an optically anisotropic material by quantifying the retardation of polarized light passing through a given sample. Each material is endowed with its own refractive index: birefringence is a characteristic property of the tissue dependent on the molecular alignment and the orientation and nature of the chemical bonds [28,29]. Had molecules and bonds formed a random organization, the refractive indices of the two rays would be equal, and the retardation would be zero. However, as the degree of alignment of polypeptide chains and chemical bonds in the collagen increases, the difference in the refractive index of the two rays increases and so does the retardation.

The method used in this research was fully reported elsewhere [30]. Three levels of optical retardation (OR) values were estimated when the collagen fibers were positioned at $\pm$ 45° relative to the ''plane of polarized light''. OR was measured in nanometers by the Senarmont method using a $\lambda/4$ compensator and monochromatic light (λ= 546nm) obtained by a narrow band-pass interference filter (Edmund Industrial Optics, Barrington, USA) [31,32].

Scanning electron microscopy (SEM) and Energy Dispersive Spectrometer (EDS) Analysis

To investigate the relationship between biomaterial particles and bone, the specimens were polished with 0.5 μm alumina to an optical finish, lightly etched with 0.1 N of HCl solution for 10 s, treated with trypsin (80 U/ml) at pH of 7.4 for 15 min at 37°C and finally sputter-coated with gold (Emitech K 550, Emitech Ltd, Ashford, Kent, UK). The samples were placed on the storage of a SEM with LaB6 (Zeiss EVO 50 XVP, Carl Zeiss SMY Ltd., Cambridge, UK), equipped with tetra solid-state BSE detector. SEM operating conditions included 30 kV accelerating voltage, 15 mm working distance, and 1.2 nA probe current. The images were captured with 20 scans using a line average technique. To perform a compositional analysis for calcium and

phosphorus concentration, an energy dispersive spectrometer (EDS; INCA, Oxford Instruments, Oxon, UK) was used.

Roughness evaluation

The surface roughness (Rs) was investigated using a confocal scanning laser microscope (CSLM), a Zeiss Axiovert 200 M with the 510META scanning module (Carl Zeiss, Jena, Germany) equipped with three lasers HeNe (543 nm, 1 mW) HeNe (633 nm, 5 mW) and Ar (458- 477- 488- 514 nm, 30 mW). Rs was determined through the triangulation method, in which a triangular network is constructed on the surface between adjacent profiles, on which the real area corresponds to the sum of the triangular elements [33].

Calculation of Rs was made considering the mean of all surface height values as:

$$R_s = \frac{1}{N_x . N_y} \sum_{i=1}^{N_x} . \sum_{j=1}^{N_y} . Z(X_i, Y_j) \qquad (3)$$

Where N_x and N_y were the numbers of pixels in X- or Y-direction.

Statistical analysis

One person performed all of the measurements. Intra-examiner variability was controlled by carrying out two measurements for each index. When the difference in the two performed readings exceeded 5% for the same index, the measurement was repeated. Statistical analysis was performed by means of a computerized statistical package (Sigma Stat 3.5, SPSS inc. Ekrath, Germany). The data were analyzed with descriptive statistics and to assess whether they had a normal distribution both Equal Variance and Normality tests were used. The difference in BIC rates was evaluated using t-test. The differences among the CFD means divided for lower, intermediary and higher values for both Nanotite and Osseotite surfaces were obtained using parametric tests after evaluating for normality and conducting the equal variance tests. One-Way ANOVA and Holm-Sidak tests were used to evaluate the overall significance and to perform all pairwise comparisons

of the mean responses, respectively. Moreover, the t-test was used to compare the means for OR in the two

investigated implant surface groups. A p value of <0.05 was considered statistically significant.

RESULTS

After a healing period of 12 months, all of the implants, which were stable and surrounded by bone, were removed.

Histologic and histomorphometric results

The histomorphometric data for both groups showed a bone growth originating from the wall of the native crestal bone that covered the ABB particles before reaching the implant surfaces (Fig. 1). In both implant groups, the deep threads of the implants (apical) still appeared to be surrounded by the structuring connective tissue (Fig. 2 and 3). The grafted particles adjacent to the implant threads were always surrounded by newly formed bone and were connected by bone bridging [34]. In some fields osteoblasts were observed in the process of apposing bone directly onto the particle surface. No gaps were present at the bone-particles interface, and the bone was always in close contact with the particles (Fig.4). The total BIC rate was 37 ± 11% for *N* implants and 48 ± 8% for *O* implants. This difference was not statistically significant (p>0.05) (Fig. 5). The histomorphometric evaluations of the specimens revealed that the highest BIC value recorded was 56% for *O* implants and 52% for *N* implants. While the lowest BIC value was 26% for *N* implants and 36% for *O* implants. In two cases, patients B and C, the BIC value of *N* implants was higher than that of the *O* implants (Table 1). Moreover, neither was an intragroup difference detected regarding the implantation site (mesial vs. distal, p>0.05) nor was any intergroup difference present for the same implantation site (p>0.05). At the level of residual crestal bone (first 4 mm of the implants), the BIC rate for *N* implants was 62.6± 0.4% while for the *O* implants, it was 54.3 ± 0.5% (Fig. 6). The difference between the two groups appeared to be statistically significant (P = 0.001) (Fig. 7).

Circularly Polarized Light Microscopy (CPLM) results

The *N* implant group, despite the lower BIC rate (-10%), showed a significantly higher CFD in the inter-threads area. The birefringence of peri-implant collagen was first evaluated as three levels of OR: lower; intermediary and higher for both groups (Table 2) than averaged for implant surface (Fig.8). The mean value

of OR was 79.8 ± 6.0 nm for the *N* group and 74.6 ± 4.6 nm for *O* group. The difference was statistically significant ($p<0.05$) (Fig. 9).

Scanning Electronic Microscopy (SEM) and Energy Dispersive Spectrometer (EDS) results

Under SEM, using backscattered electron signals, the ABB particles were visualized in white-grey due to the high atomic number (Z) of the hydroxyapatite components (i.e. Calcium, Phosphorus), while the newly formed bone appeared in dark-grey, since it also contained non-calcified organic material (lower Z). The EDS analysis was performed to determine the elemental composition along a horizontal line. Starting from the bone graft material particles and scanning towards bone along a line, calcium declined progressively in concentration, with a small peak at the edge of the particle, carbonium increased on entering bone while phosphorus concentrations remain almost constant (Fig.10).

Roughness evaluation

The *Rs* values were 0.72 ± 0.18 μm for *O* implants, 0.43 ± 0.12 μm for *N* implants and 0.31 ± 0.20 μm for bio-oss. A confocal scanning laser reconstruction showed that the surface topography of the ABB particles was much more regular than that of *N* implant surfaces (Fig.11).

DISCUSSION

The present research confirms the observation of previously published controlled animals studies by Stavropoulus *et al.* [35] who described a delayed bone formation after four months of healing in presence of ABB. The newly formed bone occupied only 12% of the total capsule space compared to the 38% of the control specimens. Carmagnola *et al.* [36,37] reported only 23% of newly formed bone after 7 months, when bio-oss was used in dogs. Also, Slotte & Lundgren [38] and Paolantonio et al [39] support that bone healing in bio-oss grafted sites is retarded, which is consistent with our observation.

Here, substantial quantitative and qualitative histological differences between experimental groups were seen. As for the BIC rate, these differences were statistically significant within the native bone, in which the *N* implants performed better than the *O* implants, suggesting that the more complex nano-topography and/or CaP deposits of the N surface may lead a more efficient osteogenetic process. These results are in accordance with Orsini *et al.* [26] who reported a statistically significant difference for the BIC rate of Osseotite and Nanotite surfaces, after a mean healing time of 2 months. The study by Goené et al. [40] pointed in the same direction, reporting, after 8-12 weeks, mean BIC rates of 45% for Nanotite and 18% for Osseotite. Therefore, the nano-textured surface performed significantly better than the micro-structured surfaces. However, these studies focused on implants that had been positioned into fully mineralized native bone, which may be the reason for such BIC values.

In the present study, when the total BIC rate of the *O* implants was compared to that of the *N* implants, no statistically significant difference was observed. Also, the bone formation process around the ABB particles was still ongoing 12 months after grafting, which raises the question whether it is premature to insert an implant contemporary to augmentation procedure.

On the other hand, the rationale of using bone graft substitutes is that the grafts serve as support for the sinus membrane and prevent its collapse, and at the same time they may also promote bone formation [41]. Our data strongly indicate that simultaneous placement of implant and ABB does not promote but rather retard the bone formation. This is consistent with the study by Telleman *et al.* [27], who compared the early peri-implant endosseous healing properties of Nanotite surfaces to Osseotite surfaces in both grafted bone and native mature bone in the maxillary regions. They concluded that the Nanotite surface improved the peri-implant endosseous healing properties in the native bone of the maxilla but did not improve the

healing properties in the bone-graft area, whose behavior may be dictated by several factors [42]. In addition, we are also in accordance with Groeneveld *et al.* [43], who reported that lamellar biomineralization occurs primarily near the maxillary host bone.

A possible explanation for the present results should be related to the relationship between blood clot formation/shrinking and biomaterials surfaces. During the implant placement, the blood vessel damage results in hemorrhage. Thus fibrin, the reaction product of thrombin and fibrinogen, is released into the healing site, allowing for the cell migration [44]. Connective tissue cell migration is concomitant with wound contraction, which usually begins around the fifth day post-wounding [45,46], and has been recognized as responsible for it [47]. This ability of cells to contract the matrix through which they migrate could possibly cause retraction of the transitory fibrin scaffold away from the implant surface. In presence of dental implants, this process may be altered: a clot detachment from the inflexible implant surface may occur leading to the lower values of BIC reported in grafted than in native bone [48,49]. Instead, bone substitute particles are subject to lower forces during the contraction phase due to their remarkable surface area and their inclusion within the clot.

Also, it is conceivable that an important role in the difference between implants and the anorganic bovine bone used in the present study may be played by mechanical features. Indeed, the ABB particles were almost completely immersed in a newly formed woven bone with some areas of well-organized osteons, which did not occur around the apical part of the implants, despite their placement simultaneous to the bone substitute material. Notwithstanding the common opinion that bone substitute materials are just to preserve the bone volume, providing proper mechanical characteristics is necessary so as to enhance mineralization [50]. During implant placement in native fully mineralized bone, the intimate direct contact between the implant surfaces and the bone-walls generates a bone strain by slight expansion. Strain signals, which are dependent on and proportional to the elasticity level of the tissue, are responsible for the features of biomineral formation. Moreover, osteoblasts and osteocytes adjacent to the implant produce various signal molecules that act locally to recruit and induce skeletogenic cells to proliferate and differentiate.

The bone biology of mineral formation is a highly complex and dynamic cell-driven process [51]. Specific strain-dependent signals are thought to control this adaptive mode of bony tissue modeling [52,53]. Peri-implant tissue formation and mineralization by osteoblasts are strongly dependent on the local mechanical

environment in the interface zone [54]. Carter and Giori [55] suggested that proliferation and differentiation of the osteoblasts responsible for peri-implant tissue formation are regulated by the local mechanical environment according to the tissue differentiation hypothesis proposed for callus formation [53]. Moreover, collagen mineralization is known to be regulated by the strains, even within an acellular environment [56]. The deposition of the collagen fibers is the initial event in the bone formation process. Collagen fibers are deposited in an irregular mosaic pattern as a woven matrix, without preferential orientation. The incorporation of mineral into the collagen matrix is a progressive process that results in bone maturation. Our finding of significantly higher values of both CFD and OR in the inter-threads spaces of *N* group is consistent with a structuring ongoing process significantly more active in the *N* implant group.

The aforementioned conditions are responsible for the many possible clinical outcomes including post-loading failures, which are thought to be ascribable to the insufficient mechanical resistance of the newly formed bone tissue. It is accepted that the dental implant survival is mainly related to the native bone quantity of the recipient sites [57], and almost independent of the biomaterial presence, the blood perfusion being of paramount importance [58,59].

All of the observations reported above may help explain the heterogeneous distribution of the BIC rate along the same implant surface. In summary, the peri-implant tissues adjacent to the augmented bone were still part of an ongoing biological adaptation process mainly consisting of densely collagen fibers not yet mineralized.

CONCLUSIONS

Consistently with the scientific literature, an increased BIC rate was noted in the native bone area when the Nanotite was compared to the Osseotite surface. However, neither of them improved the healing properties in presence of the ABB even after 12 months.

REFERENCES

1. Boyne PJ, James RA. Grafting of the maxillary sinus floor with autogenous marrow and bone. J Oral Surg 1980;38:613–6.

2. Misch CE. Maxillary Sinus Augmentation for endosteal implants: organized alternative treatment plans. Int J Oral Implantol 1987;4:49–58.

3. Watzek G. Endosseous Implants: Scientific and Clinical Aspects. Chicago: Quintessence Publishing Co, 1996 29–59, 241– 59.

4. Wallace SS, Froum SJ. Effect of maxillary sinus augmentation on the survival of endosseous dental implants as compared to the survival of implants placed in the non-grafted posterior maxilla: an evidence-based literature review. Ann Periodontol 2003; 8: 328–43.

5. Del Fabbro M, Rosano G, Taschieri S. Implant survival rates after maxillary sinus augmentation. Eur J Oral Sci 2008;116: 497–506.

6. Pjetursson BE, Tan WC, Zwahlen M, Lang NP. A systematic review of the success of sinus floor elevation and survival of implants inserted in combination with sinus floor elevation. Part I: lateral approach. J Clin Periodontol 2008;35:216–240.

7. Esposito M, Grusovin MG, Rees J, Karasoulos D, Felice P, Alissa R, Worthington HV, Coulthard P. Interventions for replacing missing teeth: augmentation procedures of the maxillary sinus. Cochrane Database Syst Rev. 2010 Mar 17;(3):CD008397.

8. Davarpanah M, Martinez H, Celletti R, Alcoforado G, Tecucianu JF, Etienne D. Osseotite implant: 3-year prospective multicenter evaluation. Clin Implant Dent Relat Res. 2001;3:111-8.

9. Lazzara RJ, Testori T, Trisi P, Porter SS, Weinstein RL. A human histologic analysis of Osseotite® and machined surfaces using implants with 2 opposing surfaces. Int J Periodontics Restorative Dent 1999;19:117-29.

10. Feldman S, Boitel N, Weng D, Kohles SS, Stach RM. Five-year survival distributions of short-length (10 mm or less) machined-surfaced and Osseotite implants. Clin Implant Dent Relat Res. 2004;6:16-23.

11. Khang W, Feldman S, Hawley CE, Gunsolley J. A multicenter study comparing dual acid-etched and machined-surfaced implants in various bone qualities. J Periodontol. 2001;72:1384–90.

12. Stach RM, Kohles SS. A meta-analysis examining the clinical survivability of machined-surfaced and Osseotite® implants in poor-quality bone. Implant Dent 2003;12:87-96.

13. Nishimura I, Huang Y, Butz F, Ogawa T, Lin L, Jake Wang C. Discrete deposition of hydroxyapatite nano-particles on a titanium implant with predisposing substrate microtopography accelerated osseointegration. Nanotechnology 2007;18:245101-10.

14. Mendes, V.C., Moineddin, R. & Davies, J.E. The effect of discrete calcium phosphate nanocrystals on bone-bonding to titanium surfaces. Biomaterials 2007; 28: 4748–4755.

15. Wennerberg A, Albrektsson T. On implant surfaces: a review of current knowledge and opinions. Int J Oral Maxillofac Implants. 2010;25:63-74.

16. Mendonca G. Mendonca DB, Simoes LG, Araùjo AL, Leite ER, Duarte WR, Aragao FJ, Cooper LF. The effects of implant surface nanoscale features on osteoblast-specific gene expression. Biomaterials 2009;30:4053– 62.

17. Vetrone F, Variola F, Tambasco de Oliveira P, Zalzal SF, Yi JH, Sam J, Bombonato-Prado KF, Sarkissian A, Perepichka DF, Wuest JD, Rosei F, Nanci A. Nanoscale oxidative patterning of metallic surfaces to modulate cell activity and fate. Nano Lett 2009;9:659–65.

18. Dalby MJ, McCloy D, Robertson M, Agheli H, Sutherland D, Affrossman S, Oreffo RO. Osteoprogenitor response to semi-ordered and random nanotopographies. Biomaterials 2006;27:2980–2987.

19. Svanborg LM, Andersson M, Wennerberg A. Surface characterization of commercial oral implants on the nanometer level. J Biomed Mater Res B Appl Biomater 2009;92:462–469.

20. Ostman PO, Wennerberg A, Albrektsson T. Immediate occlusal loading of NanoTite PREVAIL implants: a prospective 1-year clinical and radiographic study. Clin Implant Dent Relat Res. 2010;12:39-47.

21. Ostman PO, Hupalo M, del Castillo R, Emery RW, Cocchetto R, Vincenzi G, Wagenberg B, Vanassche B, Valentin A, Clausen G, Hogan P, Goenè R, Evans C, Testori T. Immediate provisionalization of NanoTite implants in support of single-tooth and unilateral restorations: one-

year interim report of a prospective, multicenter study. Clin Implant Dent Relat Res. 2010;12:e47-55.

22. Buser D, Halbritter S, Hart C, Bornstein MM, Gruetter L, Chappuis V, Belser UC. Early implant placement with simultaneous guided bone regeneration following single-tooth extraction in the esthetic zone: 12-month results of a prospective study with 20 consecutive patients. J Periodontol 2009;80:152–62.

23. Fugazzotto PA. Success and failure rates of osseointegrated implants in function in regenerated bone for 6 to 51 months: a preliminary report. Int J Oral Maxillofac Implants 2007;12:17–24.

24. Juodzbalys G, Raustia AM, Kubilius R. A 5-year follow-up study on one-stage implants inserted concomitantly with localized alveolar ridge augmentation. J Oral Rehabil 2007;34:781–789.

25. Donos N, Mardas N Chadha V. Clinical outcomes of implants following lateral bone augmentation: systematic assessment of available options (barrier membranes, bone grafts, split osteotomy). J Clin Periodontol 2008;35:173–202.

26. Orsini G, Piatelli M, Scarano A, Petrone G, Kenealy J, Piattelli A, Caputi S. Randomized, controlled histologic and histomorphometric evaluation of implants with nanometer-scale calcium phosphate added to the dual acid-etched surface in the human posterior maxilla. J Periodontol 2007; 78:209–218.

27. Telleman G, Albrektsson T, Hoffman M, Johansson CB, Vissink A, Meijer HJ, Raghoebar GM. Peri-Implant Endosseous Healing Properties of Dual Acid-Etched Mini-Implants with a Nanometer-Sized Deposition of CaP: A Histological and Histomorphometric Human Study. Clin Implant Dent Relat Res. 2010;12:153-160.

28. Wolman M, Kasten FH. Polarized light microscopy in the study of the molecular structure of collagen and reticulin. Histochemistry 1986;85:41-49.

29. Brewer DB. Differences in the fine structure of collagen and reticulin as revealed by the polarising microscope. J Path Bact 1957;74:371-385.

30. Rieppo J, Hallikainen J, Jurvelin JS, Kiviranta I, Helminen HJ, Hyttinen MM. Practical considerations in the use of polarized light microscopy in the analysis of the collagen network in articular cartilage. Microsc Res Tech 2008;71:279-87.

31. de Campos Vidal B. The part played by proteoglycans and structural glycoproteins in the macromolecular orientation of collagen bundles. Cell Mol Biol Incl Cyto Enzymol 1980;26:415–421.

32. de Campos Vidal B. Evaluation of carbohydrate role in the molecular order of collagen bundles: microphoto- metric measurements of textural birefringence. Cell Mol Biol 1986;32:527–535.

33. Brauchli LM BE, Ball J, Wichelhaus A. Roughness of enamel surfaces after different bonding and debonding procedures : An in vitro study. J Orofac Orthop 2011;72:61-7.

34. Berglundh T, Lindhe J. Healing around implants placed in bone defects treated with Bio-Oss. Clin Oral Implants Res 1997;8:117-124.

35. Stavropoulos A, Kostopoulos L, Nyengaard JR, Karring T. Deproteinized bovine bone (Bio-Oss) and bioactive glass (Biogran) arrest bone formation when used as an adjunct to guided tissue regeneration (GTR): an experimental study in the rat. J Clin Periodontol. 2003;30:636-43.

36. Carmagnola D, Berglundh T, Lindhe J. The effect of a fibrin glue on the integration of Bio-Oss with bone tissue. A experimental study in labrador dogs. J Clin Periodontol. 2002;29:377-83.

37. Carmagnola D, Adriaens P, Berglundh T. Healing of human extraction sockets filled with Bio-Oss. Clin Oral Implants Res. 2003;14:137-43.

38. Slotte C, Lundgren D. Augmentation of calvarial tissue using non-permeable silicone domes and bovine bone mineral. An experimental study in the rat. Clin Oral Implants Res. 1999;10:468-76.

39. Paolantonio M, Scarano A, Di Placido G, Tumini V, D'Archivio D, Piattelli A. Periodontal healing in humans using anorganic bovine bone and bovine peritoneum-derived collagen membrane: a clinical and histologic case report. Int J Periodontics Restorative Dent. 2001;21:505-15.

40. Goené RJ, Testori T, Trisi P. Influence of a nanometer-scalesurface enhancement on de novo bone formation on titaniumimplants: a histomorphometric study in humanmaxillae. Int J Periodontics Restorative Dent 2007; 27:211–219.

41. Pettinicchio M, Sammons R, Caputi S, Piattelli A, Traini T. Bone regeneration   in sinus augmentation procedures with calcium sulphate. Microstructure and microanaytical investigations. Aust Dent J. 2012;57:200-2006

42. Kaing L, Grubor D, Chandu A. Assessment of bone grafts placed within an oral and maxillofacial training programme for implant rehabilitation. Aust Dent J. 2011;56:406-411.

43. Groeneveld EH, van den Bergh JP, Holzmann P, ten Bruggenkate CM, Tuinzing DB, Burger EH. Mineralization processes in demineralized bone matrix grafts in human maxillary sinus floor elevations. J Biomed Mater Res 1999;48:393–402.

44. Davies JE. Understanding peri-implant endosseous healing. J Dent Educ. 2003;67:932-49.

45. Grillo HC, Potsaid MS. Studies in wound healing: IV. Retardation of contraction by local X-irradiation and observations relating to the origin of fibroblasts in repair. Ann Surg 1961;154:741-50.

46. Peacock EE. Wound repair. In: Peacock, EE, ed. Wound repair. Philadelphia: Saunders, 1984:38-55.

47. Ehrlich HP. The role of connective tissue matrix in wound healing. In: Barbul A, Pines E, Caldwell M, Hunt TK, eds. Growth factors and other aspects of wound healing: biological and clinical implications. New York: Liss, 1988:243-58.

48. Benlidayi ME, Kürkcü M, Oz IA, Sertdemir Y. Comparison of two different forms of bovine-derived hydroxyapatite in sinus augmentation and simultaneous implant placement: an experimental study. Int J Oral Maxillofac Implants. 2009;24:704-11.

49. Telleman G, Albrektsson T, Hoffman M, Johansson CB, Vissink A, Meijer HJ, Raghoebar GM. Peri-Implant Endosseous Healing Properties of Dual Acid-Etched Mini-Implants with a Nanometer-Sized Deposition of CaP: A Histological and Histomorphometric Human Study Clin Implant Dent Relat Res. 2010;12:153-60.

50. Park JB. Radiographic follow-up evaluation of sinus augmentation with deproteinized bovine bone and implant installation after loading. Indian J Dent Res. 2010;21:603-5

51. Wiesmann HP, Joos U, Meyer U. Biological and biophysical principles in extracorporal bone tissue engineering. Part II. Int J Oral Maxillofac Surg 2004;33:523–530.

52. Duncan RL, Turner CH. Mechanotransduction and the functional response of bone to mechanical strain. Calcif Tissue Int 1995;57:344–358.

53. Distraction osteogenesis based on the Utah paradigm. In: Jensen OT, ed: Alveolar Distraction Osteogenesis. Illinois, USA: Quintessence Publisher 2002.

54. Pillar RM. Quantitative evaluation of the effect of movement at a porous coated implant-bone interface. In: Davies JE, ed: The Bone–Biomaterial Interface. Toronto: University of Toronto Press 1991.

55. Carter DR, Giori NJ. Effect of mechanical stress on tissue differentiation in the bony implant bed. In: Davies JE, ed: The Bone–biomaterial Interface. Toronto: Univerity of Toronto Press 1991: 367.

56. Fratzl P, Schreiber S, Klaushofer K. Bone mineralization as studied by small-angle x-ray scattering. Connect Tissue Res 1996:34: 247–254.

57. Lambert F, Lecloux G, Rompen E. One-step approach for implant placement and subantral bone regeneration using bovine hydroxyapatite: a 2- to 6-year follow-up study. Int J Oral Maxillofac Implants. 2010;25:598-606.

58. Cricchio G, Sennerby L, Lundgren S. Sinus bone formation and implant survival after sinus membrane elevation and implant placement: a 1- to 6-year follow-upstudy. Clin Oral Implants Res. 2011;22:1200-12.

59. Thor A, Sennerby L, Hirsch JM, Rasmusson L. Bone formation at the maxillary sinus floor following simultaneous elevation of the mucosal lining and implant installation without graft material: an evaluation of 20 patients treated with 44 Astra Tech implants. J Oral Maxillofac Surg. 2007;65(7 Suppl 1):64-72.

FIGURE LEGENDS

Figure 1. *O* implants **(a-a1)** and *N* implants (**b-b1**), both implant groups were partially osseointegrated. Along the apical parts of the implant surfaces (regenerated/augmented bone area) only focal osseointegration areas were seen. Original magnification x 12. Acid Fuchsine- azur II staining.

Figure 2. Map reconstruction showing apical threads of one *N* implant. The Bio-oss particles (BOp) appeared surrounded and bridged by newly formed bone (NB). Between threads densely collagen fiber were present (**). Original magnification x 50. Acid Fuchsine- azur II staining.

Figure 3. Map reconstruction showing apical threads of one *O* implant. The Bio-oss particles (**) appeared surrounded and bridged by newly formed bone (NB). White arrows show newly formed bone (NB) between threads in contact with implant surface. Original magnification x 50 under CPL. Acid Fuchsine- azur II staining.

Figure 4. Around the implant threads (I) the Bio-oss particles (BOp) were surrounded and bridged by newly formed bone (NB). Original magnification x 100. Acid Fuchsine- azur II staining.

Figure 5. Graph of total BIC rate for *O* and *N* implants. No statistically significant difference was present (Unpaired t-test)

Figure 6. Images at x 100 of *N* (a) and *O* (b) implants under CPL at crestal level. The newly formed bone, facing the native bone, along the implant surfaces is more mature with a higher BIC in (a) than in (b).

Figure 7. Graph of BIC rate in native bone for *O* and *N* implants. A statistically significant difference was present (Unpaired t-test).

Figure 8. Image showing *N* implant (a) and *O* implant (b) at 100 x. (I) implant threads at apical level; (**) mineralized bone; (*) scanned areas for retardations intensity. Graphical representation of Red Green and Blue wavelength intensity vs distance for *N* implants (a1) and *O* implants (b1).

Figure 9. Graph showing the birefringence of peri-implant collagen fibers. The difference in the mean values of *O* and *N* groups is greater than would be expected by chance. Statistical significance (p = 0.006) was assessed by the Unpaired t-test.

Figure 10. In (a) SEM image using backscattered electron signals of augmented bone tissue. The biomaterial particles appeared in white-grey due to the high atomic number of the hydroxyapatite, while the newly formed bone appeared in dark-grey. Rectangle b was imaged at higher magnification in (b). In (b) the Biomaterial appeared in white-gray while the newly formed bone in dark-gray. EDS analysis was performed at the interface along the black line to determine the elemental composition. In (c) are shown the colored lines spectra for each element which indicates the concentrations of carbon (red); Calcium (green) and Phosphorus (blue). Calcium declined in concentration, the decrease continuing on entering the bone, with a small peak at the edge of the particle. Carbon concentration increased on entering bone while Phosphorus concentrations remain almost constant.

Figure 11. Surface map reconstructions of roughness of *N* surface (a) and ABB (b).
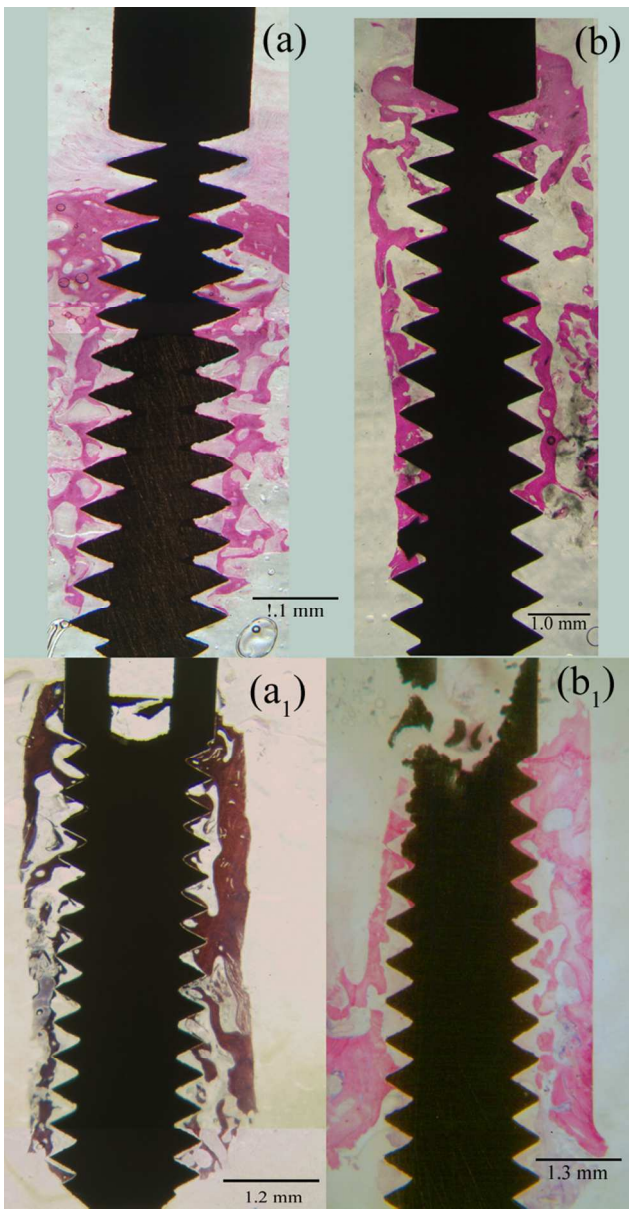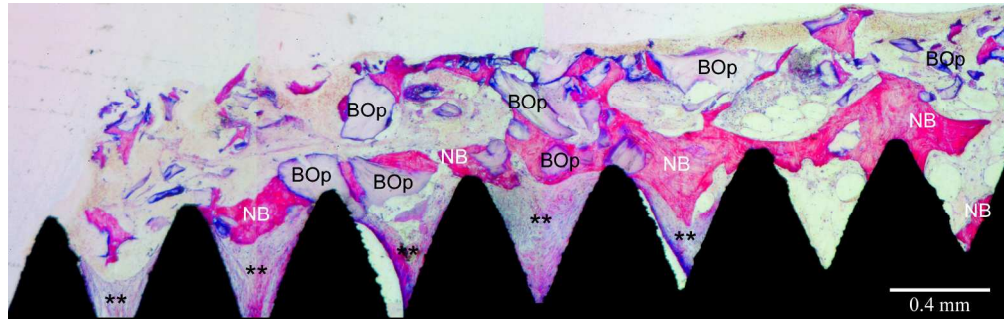
61x118mm (300 x 300 DPI)

211x66mm (300 x 300 DPI)

1
2
3
4
5
6
7
8
9
10
11
12
13
14
15
16
17
18
19
20
21
22
23
24
25
26
27
28
29
30
31
32
33
34
35
36
37
38
39
40
41
42
43
44
45
46
47
48
49
50
51
52
53
54
55
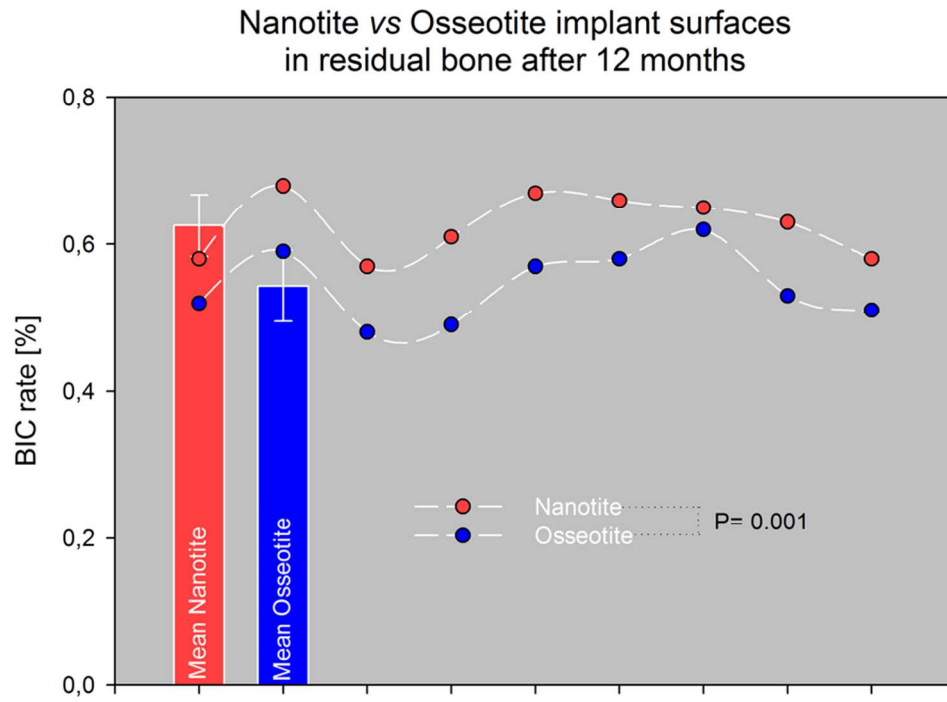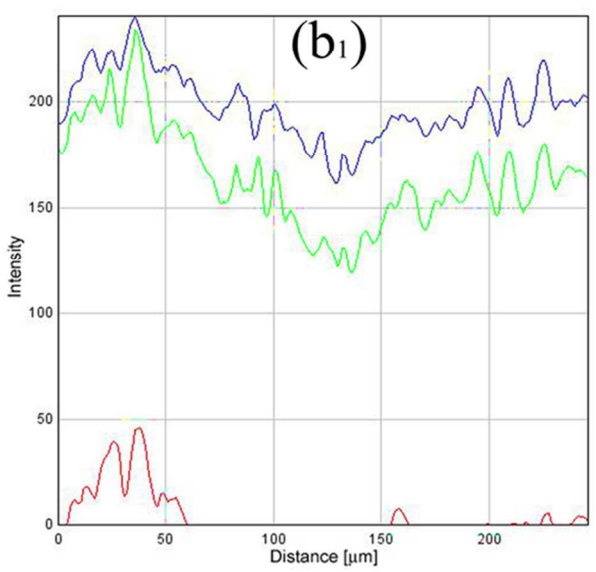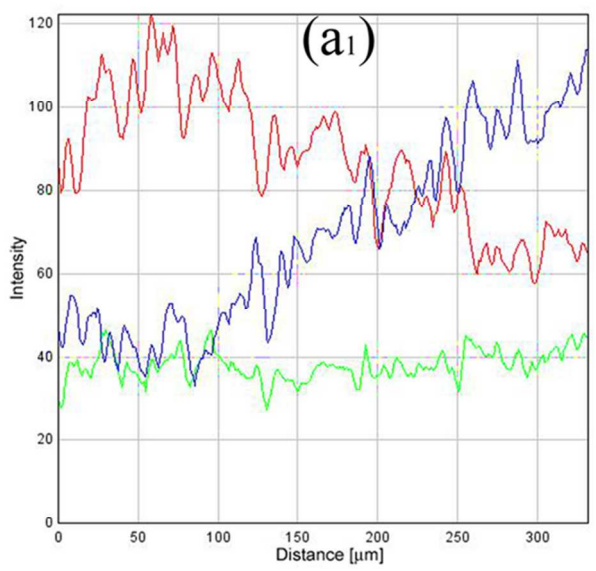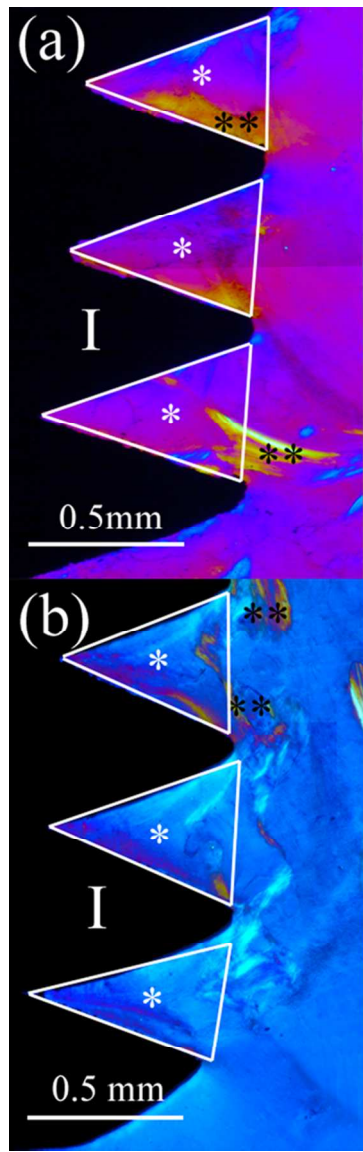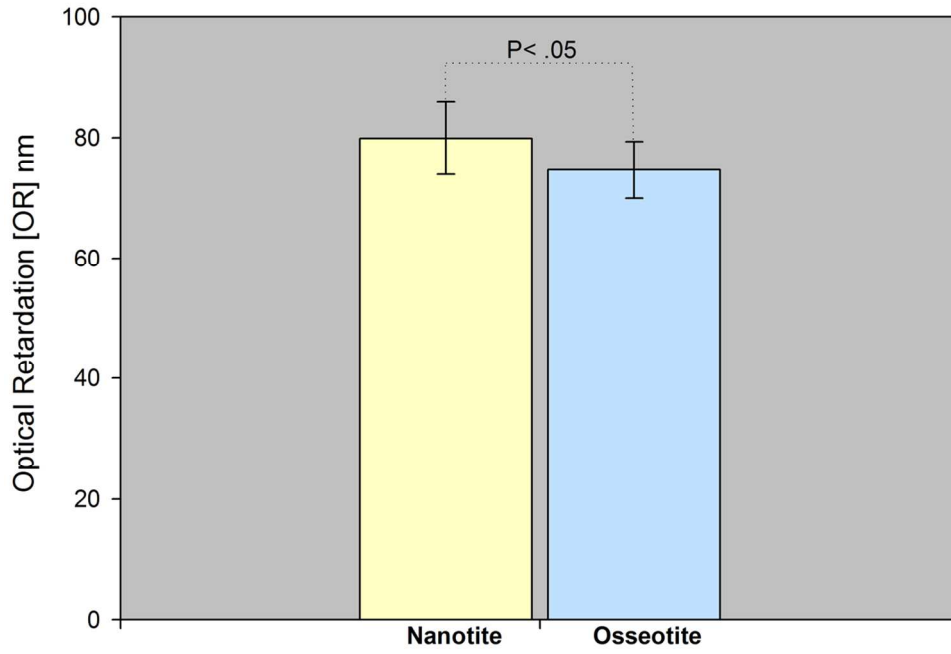56
57
58
59
60

135x53mm (300 x 300 DPI)

167x98mm (300 x 300 DPI)

163x121mm (300 x 300 DPI)

Nanotite *vs* Osseotite implant surfaces in residual bone after 12 months
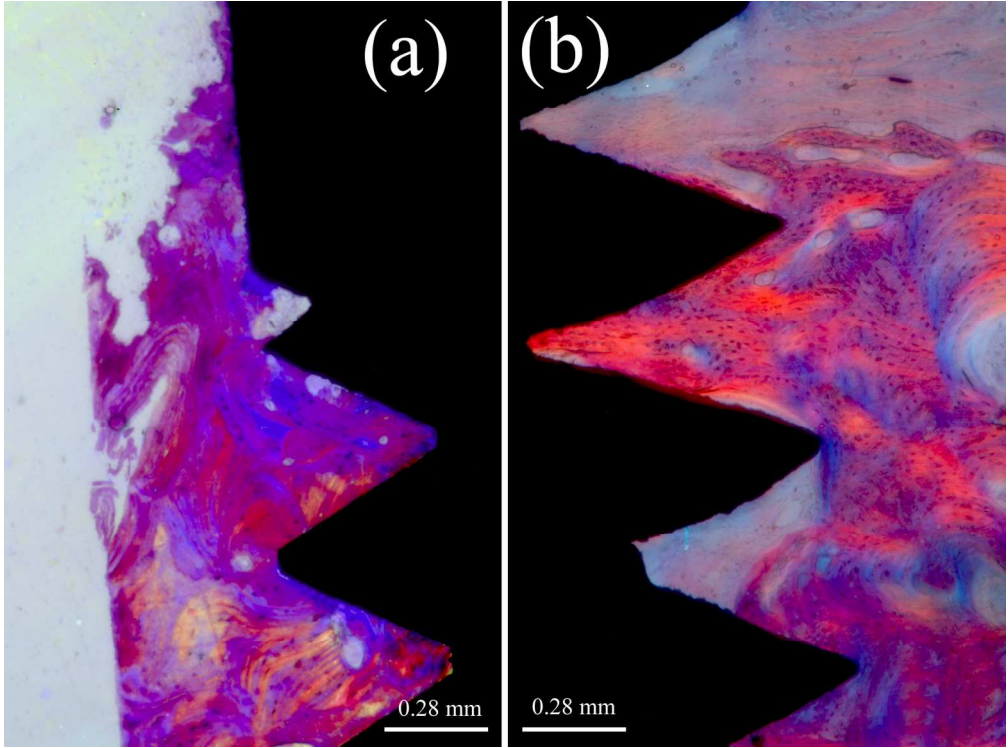
86x63mm (300 x 300 DPI)

1
2
3
4
5
6
7
8
9
10
11
12
13
14
15
16
17
18
19
20
21
22
23
24
25
26
27
28
29
30
31
32
33
34
35
36
37
38
39
40
41
42
43
44
45
46
47
48
49
50
51
52
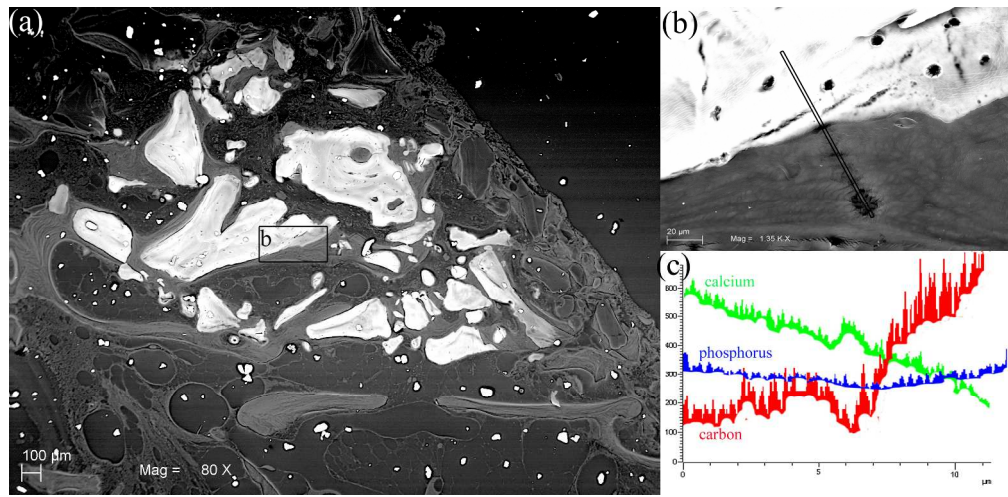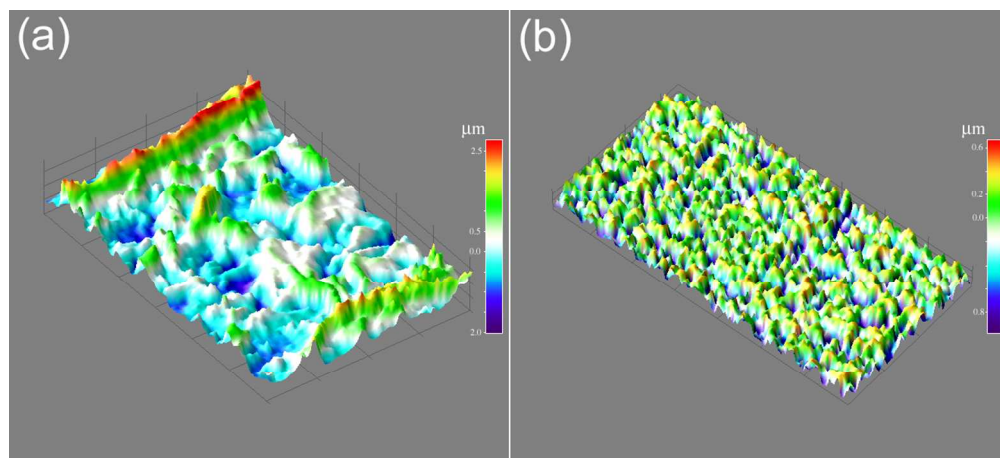53
54
55
56
57
58
59
60

86x98mm (300 x 300 DPI)

1
2
3
4
5
6
7
8
9
10
11
12
13
14
15
16
17
18
19
20
21
22
23
24
25
26
27
28
29
30
31
32
33
34
35
36
37
38
39
40
41
42
43
44
45
46
47
48
49
50
51
52
53
54
55
56
57
58
59
60

115x81mm (300 x 300 DPI)

1
2
3
4
5
6
7
8
9
10
11
12
13
14
15
16
17
18
19
20
21
22
23
24
25
26
27
28
29
30
31
32
33
34
35
36
37
38
39
40
41
42
43
44
45
46
47
48
49
50
51
52
53
54
55
56
57
58
59
60

266x130mm (300 x 300 DPI)

111x50mm (300 x 300 DPI)

1
2
3   Table 1
4
5
6
7
8

Patient	BIC Nanotite^{TM} (Surface)	BIC Osseotite® (Surface)
A1	34% (D)	53% (M)
A2	44% (M)	49% (D)
B	49% (M)	40% (D)
C	37% (D)	36% (M)
D	26% (D)	53% (M)
E1	24%(M)	37% (D)
E2	21% (D)	56% (M)
F	52% (D)	55% (M)
G	44% (D)	49% (M)
MEAN	37%	48%
SD	0.113002	0.07844

Table 2

Birefringence variability in collagen fibers detected by optical retardation (nm)					
Nanotite			*Osseotite*		
Mean	**SD**	**n**	**Mean**	**SD**	**n**
Lower 64,767	4,010	6	61,267	1,366	6
Intermediary 78,167	1,381	6	72,217	1,814	6
Higher 96,683	3,131	6	90,367	1,469	6